JMEPEG (2012) 21:197–201
DOI: 10.1007/s11665-011-9879-2

1059-9495/$19.00

Effects of Two Different Dynamic Loading Conditions on Spall and Damage of 7075 Aluminum Alloy

Yang Yang, Xiaoming Li, Chengyuan Xu, Liansheng Zhang, Qingming Zhang, and Xiaole Tong

(Submitted November 25, 2010; in revised form January 21, 2011)

The fracture behaviors of the 7075 aluminum alloy under two different dynamic loading conditions are investigated by means of a light-gas gun. The fracture surfaces obtained in the spall test are compared to the fracture surfaces obtained with a blunt projectile struck to the aluminum alloy plate. Optical and scanning electron microscopes are used in the investigation. For the plate-impact test, spall of the target was attributed to intergranular fracture caused by the tensile stress. The fracture behavior during projectile penetration is complex and consists of several fracture modes in addition to that the fracture is also of dynamic character. The penetration process of aluminum alloy target included: plugging stage, the microcracks nucleation stage, and the final tensile fracture stage. Mixed intergranular brittle/ductile fracture was observed, and brittle fracture played a dominate role.

Keywords aluminum, fracture, impact and ballistic

1. Introduction

Spall fracture is one of shock-induced dynamic fracture phenomena (Ref 1, 2). The plate-impact test is the most widely used in the high-rate experiments. The gas gun (Ref 3-6), electro-explosive devices (Ref 7), and laser techniques (Ref 8) are used to launch the flyer plate in a large number of experiments. In recent years, spall mechanism is extensively investigated. Hu et al. (Ref 8) studied the spallation and fracture of tungsten by laser-induced stress waves. Bai et al. (Ref 9) presented a model of statistical microdamage evolution to spall fracture. Furnish et al. (Ref 10) investigated spall of tantalum from 7 to 13 GPa.

Spall is also observed in the process of penetration. Tanaka et al. (Ref 11) investigated the high-speed penetration of a projectile into aluminum alloys at low temperatures. Dikshit et al. (Ref 12) investigated the influence of plate hardness on the ballistic penetration of thick steel plates and presented the incidence and extent of adiabatic shear band formation and plate spall.

7075 aluminum alloy belongs to the Al-Zn-Mg-Cu series high strength and toughness alloy, which is one of the most important engineering alloys and widely used in aircraft structures (Ref 13-16). Several investigations have studied the fracture behaviors of 7075 aluminum alloy under different loading conditions (Ref 17-20). The effects of two different dynamic loading conditions on spall and damage of 7075 aluminum alloy were investigated in the present work.

Yang Yang, Xiaoming Li, Chengyuan Xu, and **Xiaole Tong**, School of Materials Science and Engineering, Central South University, Changsha 410083, Hunan, People's Republic of China; and **Liansheng Zhang** and **Qingming Zhang**, State Key Laboratory of Explosion Science and Technology, Beijing 100081, People's Republic of China. Contact e-mail: xiaomingguowei@yahoo.com.cn.

2. Experimental Procedure

7075 aluminum alloy is investigated in the present work. The heat-treated state of the aluminum alloy was the T651, which was solid solution followed by plastic deformation with strain about 1-3%, and then aged at 120 °C/24 h. The chemical composition of 7075 aluminum alloy is listed in Table 1.

The dynamic loading tests were carried out on a light-gas gun at the State Key Laboratory of Explosion Science and Technology. The two loading conditions were plate-impact and penetration test, respectively. The velocities of the flyer plate and projectile were measured using electrical contact pins placed between the target block and the light-gas gun. The diameter and thickness of aluminum alloy target were 60 and 8 mm. For the plate-impact test, the flyer plate, of 53 mm in diameter and 3 mm thick, made of copper was glued on the top of a sabot made of PMMA and PVC. The total mass of the flyer plate and sabot was 215 g, and the velocity was 450 m/s. For the penetration experiment, the projectile, of 10 mm in diameter, and 30 mm long, made of 603 armor steel was glued on the top of a sabot. The total mass of the projectile and sabot was 223 g, and the velocity was 470 m/s.

The specimens for investigation were cut from the recovered targets. The chemical attack for 7075 aluminum alloy was a solution of HF 1 mL, HNO_3 2.5 mL, HCl 1.5 mL, and H_2O 95 mL. The metallographic analysis was made by means of POLYVAR-MET optical microscopy (OM) and SIRION200 field emission scanning electron microscope (SEM) which was equipped with Gensis60 energy dispersive spectrometer (EDS) and operated at 10 and 15 kV.

3. Experimental Results and Analysis

3.1 The Macroscopic Characteristics of Fragments

For plate-impact test, Fig. 1 is the distance-time diagram of the wave process after impact of the flyer plate on the target.

The impact causes shock waves to propagate in the flyer and target plates away from the impact face. Reflection of the waves occurs at the free surfaces. The two release shock waves meet inside the target to produce a plane of tension. The target will fail at the plane and separate into two pieces if the amplitude of the tensile wave exceeds the spall strength of the material (Ref 21). The reciprocal of the oblique line slope is the wave velocity (Fig. 1). For the wave velocity of aluminum alloy $c_+ = 5328$ m/s, the wave velocity of copper $c_- = 3940$ m/s (Ref 1), the coordinate where the two release shock waves meet x_0 is 3.34 mm, close to the measured value of the remaining target thickness 3.62 mm. The macrofracture surface is shown in Fig. 2(a) and (b). The black residue on the fracture surface is the buffer fiber.

Table 1 Chemical composition (in wt.%) of 7075 aluminum alloy

Zn	Mg	Cu	Cr	Mn	Fe	Si	Al
5.72	2.19	1.54	0.25	0.04	0.21	0.19	Bal.

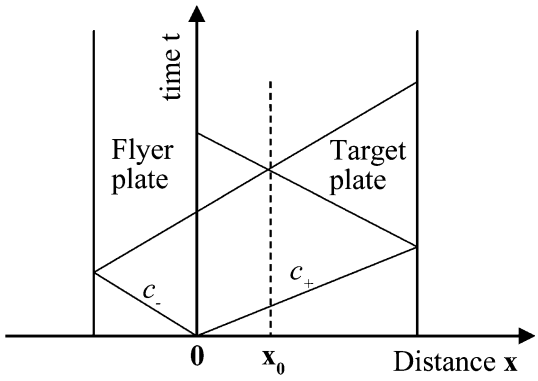

Fig. 1 The distance-time diagram of the wave process (Ref 2)

The figures of penetrated target are shown in Fig. 2(c) and (d), which show the front surface, where the projectile enters the target, and the rear surface, where the projectile exits. It could be seen that fragmentation took place during impact, indicating a quasi-brittle behavior of the alloy. A plug with height less than the plate thickness was ejected from the target. The fracture behavior for the two loading conditions is significantly different. The differences in the primary deformation modes for the two cases, namely shear plugging for the penetration test and spall fracture for the plate-impact test.

3.2 Analysis of Microstructure

The metallographic of the cross section of the target plate after plate impact is shown in Fig. 3(a). The microstructure (ND) is not significantly changed and still coarse recrystallized matrix microstructure. The grains of the longitudinal section were elongated as shown in Fig. 3(b). It could be seen that the

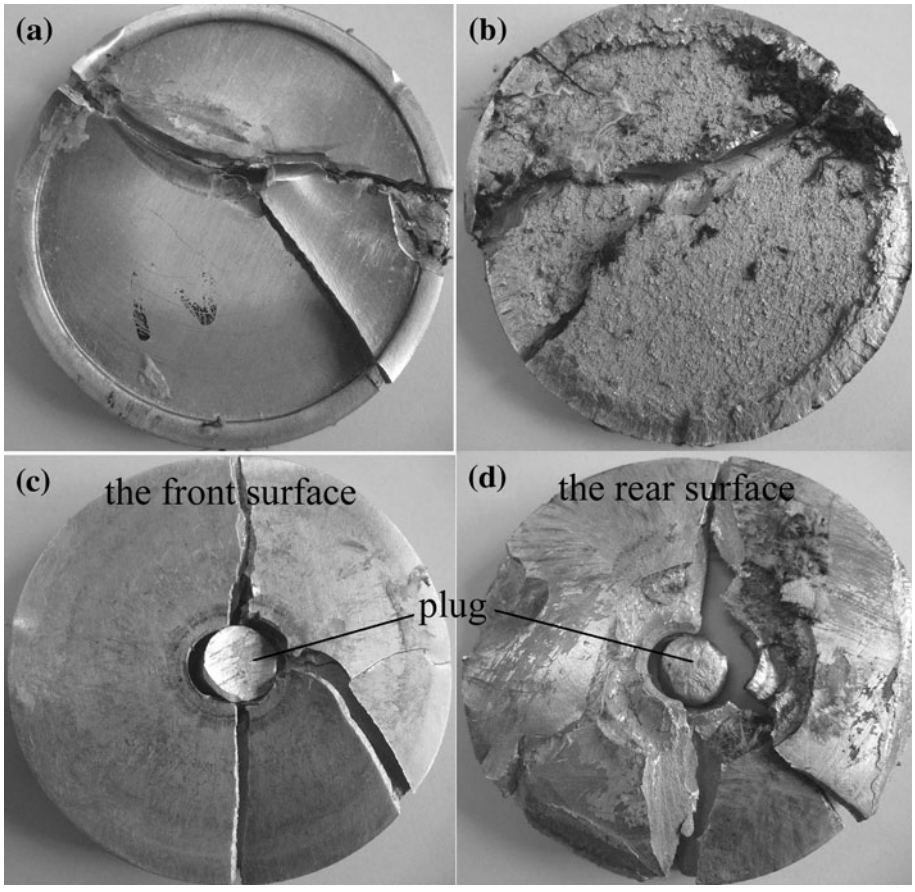

Fig. 2 Macromorphology of recovered specimens: (a) and (b) plate-impact, (c) and (d) penetration

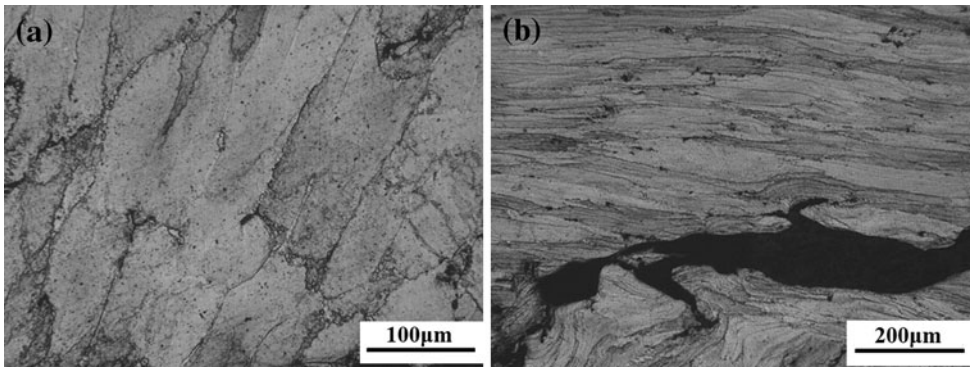

Fig. 3 Optical microstructure of plate-impacted specimens: (a) matrix and (b) cracks

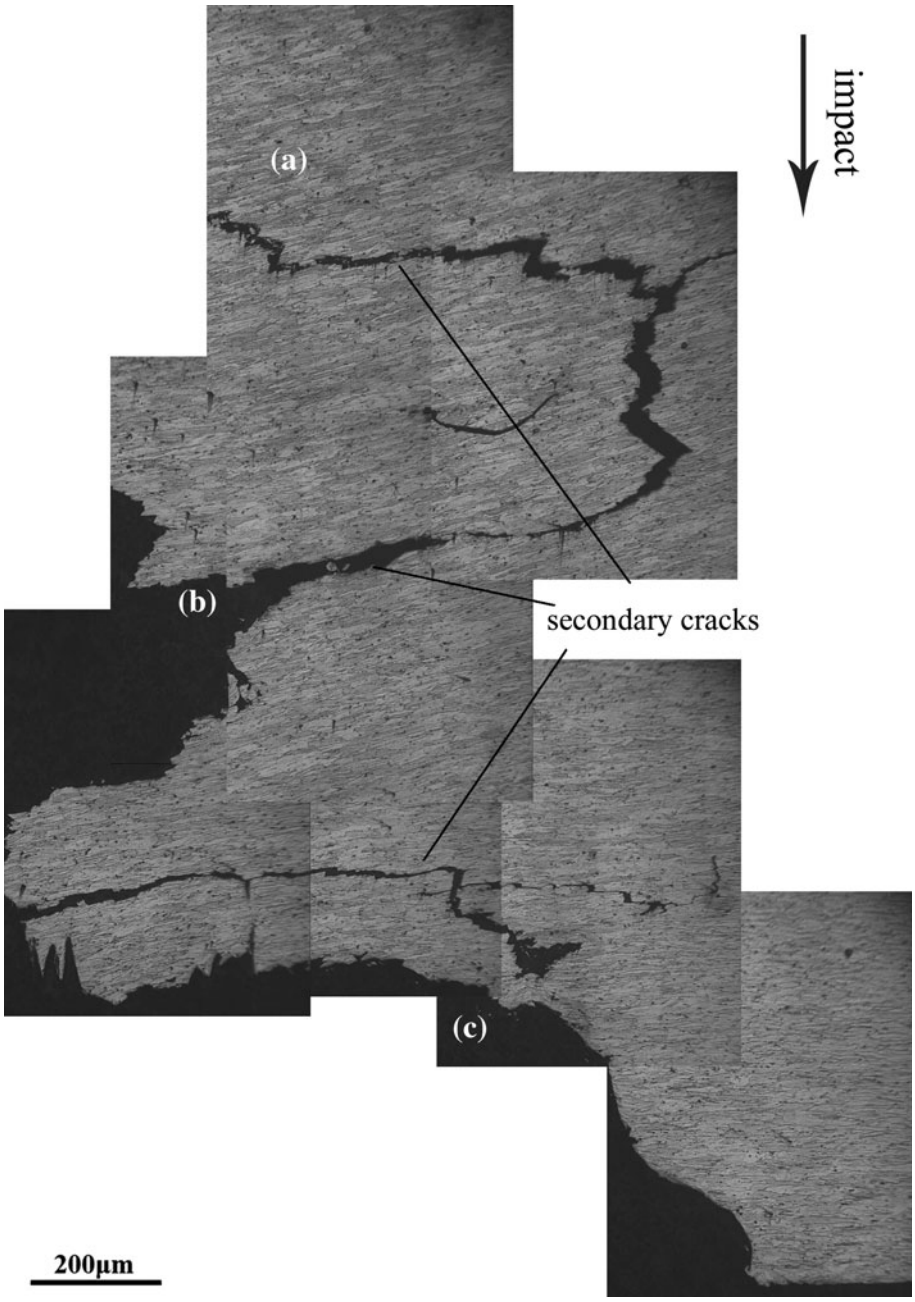

Fig. 4 Optical microstructure of radial section of the penetrated target

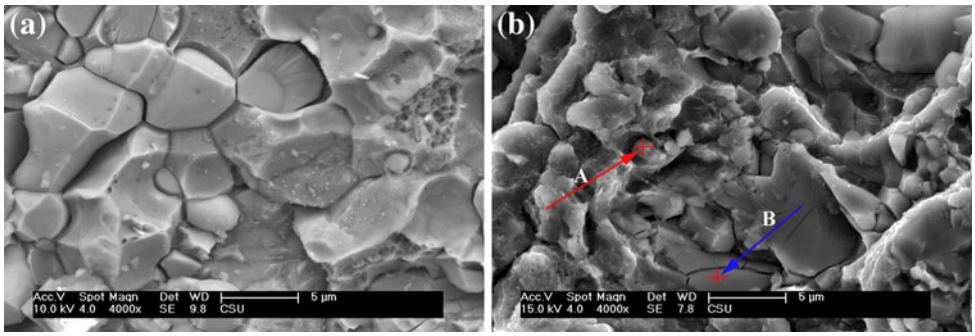

Fig. 5 SEM fracture morphologies of plate-impacted targets

Table 2 Chemical composition of particle A and B (Fig. 5)

	Element	Zn	Mg	Al	Cr	Fe	Cu
A	wt.%	3.96	1.27	66.32	5.2	13.81	7.53
	at.%	1.96	1.7	79.48	3.23	8.0	3.83
B	wt.%	4.47	0.79	68.25	···	18.94	7.55
	at.%	2.21	1.05	81.9	···	10.98	3.85

··· not detected

cracks propagated along the grain boundaries. Cracks nucleate at many separate sites, which is a typical feature of dynamic fracture (Ref 1).

The fracture behavior during projectile penetration is complex and consists of several fracture modes in addition to that the fracture is also of dynamic character. The microstructure of the radial section of the penetrated target is shown in Fig. 4. The blunt projectile results in shear deformation and the secondary cracks are normal to the penetration channel. The process of the penetration includes three stages: plugging stage, microcracks nucleation stage, and final tensile fracture stage. Shear deformation occurred in the target in the plugging stage (zone A in Fig. 4). At the microcracks nucleation stage (zone B in Fig. 4), the impact caused shock waves to propagate in the flyer and target plates after impact. Rarefaction fans were generated when these initial waves were reflected at the outer free boundaries. The cracks parallel to the rear surface were formed due to spall. It was difficult to perforate the target for the blunt projectile. The large kinetic energy forced the projectile to push the target material forward, and then a bulge at the rear surface was formed, which caused the aluminum alloy around to flow toward the crater. There was shear stress inside the target parallel to the initial spall cracks. At the final tensile fracture stage (zone C in Fig. 4), the tensile stress played a dominate role. The bulge was pulled away from the target, when the tensile stress exceeded the tensile strength of 7075 aluminum alloy, and the final tensile fracture was formed. It can be seen near the point C of Fig. 4 that the crack propagates along the grain boundary, and there are fractured grains. It can be considered that the fracture of the penetration is mixed intergranular brittle/ductile fracture.

3.3 The Microscopic Characteristics of Fracture

For the plate-impact test, SEM photographs of spall fracture are shown in Fig. 5(a). The rock candy pattern was observed, which is a kind of brittle fracture structure due to intergranular cracking. It can be inferred that both the particle A and B of Fig. 5(b) are Al_7CuFe phase particles by the ratio of the percentage contents of the elements in Table 2. There are a large number of dislocations on the interface of the particles and matrix when plastic deformation occurs, which induces stress concentration. Microvoids/microcrack may nucleate at the interface when the stress concentration increases to a certain degree. The grain boundaries or the regions in the vicinity of the grain boundaries are weak areas because of the precipitation free zones adjacent to the grain boundary and the grain boundary particles. The grain boundary is embrittled by the precipitates and impurities, so the grain boundary strength decreases. In addition, nucleation and coalescence of microvoids at the grain boundary causes the cohesion of the grain boundary to decrease. Therefore, the grain boundary strength is less then the intragranular strength. This is one of major factors leading to intergranular fracture.

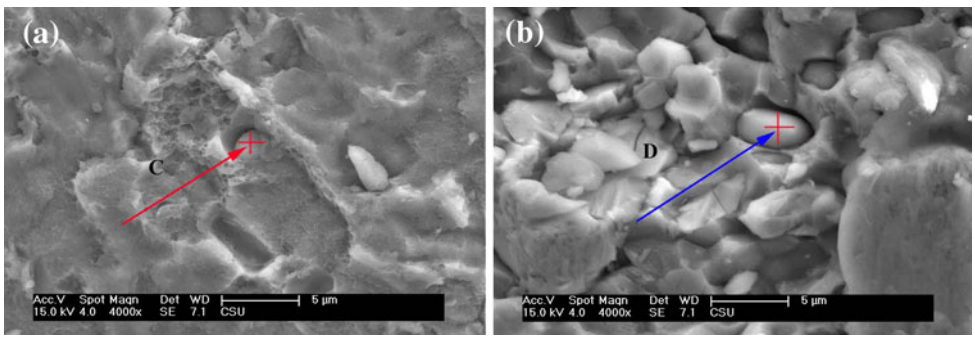

Fig. 6 SEM fracture morphologies of penetration fracture

Table 3 Chemical composition of point A and B (Fig. 6)

	Element	Zn	Mg	Al	Si	Cu
A	wt.%	3.0	34.58	47.14	15.27	···
	at.%	1.22	37.84	46.48	14.47	···
B	wt.%	···	16.24	41.93	···	41.84
	at.%	···	23.19	53.95	···	22.86

··· not detected

The SEM photographs of the fracture in the penetration test are shown in Fig. 6. There are a few small dimples. Mixed intergranular brittle/ductile fracture is observed, and brittle fracture plays a dominate role. It can be inferred that particle C of Fig. 6(a) is Mg_2Si phase particle and particle D of Fig. 6(b) is S phase ($CuMgAl_2$) particle by the ratio of the percentage contents of the elements in Table 3. During the process of deformation, these coarse second phase particles became the source of cracks, and finally lead to the fracture of materials. Therefore, spall fracture of penetration is mixed intergranular brittle/ductile fracture.

4. Conclusions

The impact tests on the 7075 aluminum alloy plates using flyer plates and blunt projectiles indicated that the alloy was like a quasi-brittle material under dynamic impact loading conditions. The differences in the primary deformation modes for the two cases, namely shear plugging for the penetration test and spall fracture for the plate-impact test. For the plate-impact test, spall fracture in the target was attributed to intergranular fracture caused by tensile stress.

The fracture behavior during projectile penetration is complex and consists of several fracture modes in addition to that the fracture is also of dynamic character. The penetration process of aluminum alloy target included: plugging stage, the microcracks nucleation stage, and the final tensile fracture stage. Fracture of penetration is mixed intergranular brittle/ductile fracture, and brittle fracture played a dominate role.

Acknowledgments

This work was supported by the project National Nature Science Foundation of China (No. 50971134), the project of Pre-research Fund of the PLA General Armament Department (No. 9140A12011610BQ1901), and the key project of State Key Laboratory of Explosion Science and Technology (No. KFJJ09-1).

References

1. M.A. Meyers, *Dynamic Behavior of Materials*, Wiley-Interscience, New York, 1994
2. T.H. Antoun, L. Seaman, D.R. Curran, Gl. Kanel, S.V. Razorenov, and A.V. Utkin, *Spall Fracture*, Springer, New York, 2003
3. P. Chevrier and J.R. Klepaczko, Spall Fracture: Mechanical and Microstructural Aspects, *Eng. Fract. Mech.*, 1999, **63**, p 273–294
4. S.J. Bless, K. Tarcza, R. Chau, E. Taleff, and C. Persad, Dynamic Fracture of Tungsten Heavy Alloys, *Int. J. Impact Eng.*, 2006, **33**, p 100–108
5. Y. Yu, D. Chen, H. Tan, H. Wang, S. Xie, and M. Zhang, Spall Investigations for LY12 Al Using Triangular Waves, *Int. J. Impact Eng.*, 2007, **34**, p 395–404
6. R.I. Barabash, G.E. Ice, M. Kumar, J. Ilavsky, and J. Belak, Polychromatic Microdiffraction Analysis of Defect Self-Organization in Shock Deformed Single Crystals, *Int. J. Plast.*, 2009, **25**, p 2081–2093
7. Y.C. Zhou, Z.P. Duan, and X.H. Yan, Thermal Stress Wave and Spallation Induced by an Electron Beam, *Int. J. Impact Eng.*, 1997, **19**, p 603–614
8. L. Hu, P. Miller, and J. Wang, High Strain-Rate Spallation and Fracture of Tungsten by Laser-Induced Stress Waves, *Mater. Sci. Eng. A.*, 2009, **504**, p 73–80
9. Y.L. Bai, J. Bai, H.L. Li, F.J. Ke, and M.F. Xia, Damage Evolution, Localization and Failure of Solids Subjected to Impact Loading, *Int. J. Impact Eng.*, 2000, **24**, p 685–701
10. M.D. Furnish, L.C. Chhabildas, W.D. Reinhart, W.M. Trott, and T.J. Vogler, Determination and Interpretation of Statistics of Spatially Resolved Waveforms in Spalled Tantalum from 7 to 13 GPa, *Int. J. Plast.*, 2009, **25**, p 587–602
11. K. Tanaka, M. Nishida, and N. Takada, High-Speed Penetration of a Projectile into Aluminum Alloys at Low Temperatures, *Int. J. Impact Eng.*, 2006, **33**, p 788–798
12. S.N. Dikshit, V.V. Kutumbarao, and G. Sundararajan, The Influence of Plate Hardness on the Ballistic Penetration of Thick Steel Plates, *Int. J. Impact Eng.*, 1995, **16**, p 293–320
13. W.-S. Lee, W.-C. Sue, C.-F. Lin, and C.-J. Wu, The Strain Rate and Temperature Dependence of the Dynamic Impact Properties of 7075 Aluminum Alloy, *J. Mater. Process. Technol.*, 2000, **100**, p 116–122
14. Y. Yang, Y. Zeng, and Z.W. Gao, Numerical and Experimental Studies of Self-organization of Shear Bands in 7075 Aluminium Alloy, *Mater. Sci. Eng. A*, 2008, **496**, p 291–302
15. Y. Yang, Y. Zeng, D.H. Li, and M. Li, Damage and Fracture Mechanism of Aluminium Alloy Thick-Walled Cylinder Under External Explosive Loading, *Mater. Sci. Eng. A*, 2008, **490**, p 378–384
16. Y. Yang, X.M. Li, S.W. Chen, Q.M. Zhang, F. Jiang, and H.G. Zheng, Effects of Pre-notches on the Self-Organization Behaviors of Shear Bands in Aluminum Alloy, *Mater. Sci. Eng. A*, 2010, **527**, p 5084–5091
17. E. El-Magd and M. Brodmann, Influence of Precipitates on Ductile Fracture of Aluminium Alloy AA7075 at High Strain Rates, *Mater. Sci. Eng. A*, 2001, **307**, p 143–150
18. J.A. Loya and J. Fernández-Sáez, Three-Dimensional Effects on the Dynamic Fracture Determination of Al 7075-T651 Using TPB Specimens, *Int. J. Solids Struct.*, 2008, **45**, p 2203–2219
19. T. Børvik, O.S. Hopperstad, and K.O. Pedersen, Quasi-Brittle Fracture During Structural Impact of AA7075-T651 Aluminium Plates, *Int. J. Impact Eng.*, 2010, **37**, p 537–551
20. K.O. Pedersen, T. Børvik, and O.S. Hopperstad, Fracture Mechanisms of Aluminium Alloy AA7075-T651 Under Various Loading Conditions, *Mater. Des.*, 2011, **32**, p 97–107
21. A.K. Zurek, W.R. Thissell, J.N. Johnson, D.L. Tonks, and R. Hixson, Micromechanics of Spall and Damage in Tantalum, *J. Mater. Process. Technol.*, 1996, **60**, p 261–267